AAS 22-685

RESILIENCE OF ORBITAL INSPECTIONS TO PARTIAL LOSS OF CONTROL AUTHORITY OF THE CHASER SATELLITE

Jean-Baptiste Bouvier[*], Himmat Panag[†], Robyn Woollands[‡], and Melkior Ornik[§]

The growing demand for orbital inspections can only be met if these missions guarantee not to endanger the target satellite. To address this issue we study how to make the chaser satellite resistant to a partial loss of control authority over its thrusters. This malfunction is characterized by some thrusters of the spacecraft firing in an uncontrolled and thus possibly undesirable manner. Because of actuation delays, these undesirable thrust inputs cannot be canceled in real-time. Instead, we first use resilience theory to show that a sufficiently overactuated spacecraft can still reach any location even after losing control of a thruster. We then calculate the safety distance ensuring that the malfunctioning chaser satellite will not breach the keep-out sphere around the target satellite. We employ a convex solver to generate a safe minimal-fuel reference trajectory to perform the inspection mission. Relying on state prediction, adaptive trajectory tracking and PID control the malfunctioning spacecraft is then able to follow the reference trajectory. We thus demonstrate that an orbital inspection mission can be carried out safely by a spacecraft enduring actuation delay and a loss of control authority over one of its thrusters.

INTRODUCTION

With an increase in the number of active satellites, there is a growing demand for on-orbit satellite inspection, e.g., to assess damage on satellites, improve the safety of astronauts, or even enforce the ban of space weapons.[1–4] The importance of satellite inspection is also reflected by the creation of spacecrafts entirely dedicated to on-orbit inspections, like the robot Laura from the Rogue Space Systems Corporations[*]. Partly inspired by the on-orbit servicing Restore-L mission,[5] our scenario of interest consists in an *orbital inspection* of a satellite by a spacecraft that completes a full revolution around the target satellite.

Following an on-board computer error, the inspecting spacecraft endures a *loss of control authority*[6] over one of its thrusters, similarly to what happened to the Nauka module when docked to the International Space Station.[7] This malfunction consists in one of the thrusters producing uncontrolled and thus possibly undesirable thrust with its full capability. Then, the undesirable inputs can have a magnitude similar to the controls, which renders robust control practically useless due to its conservatism.[8] Other safety methods for close proximity operations with respect to thruster failures often consider that malfunctioning thrusters are completely disabled.[9,10] Such a malfunction

[*]PhD Candidate, Department of Aerospace Engineering, University of Illinois Urbana-Champaign, USA, AAS Member.
[†]MS Student, Department of Aerospace Engineering, University of Illinois Urbana-Champaign, USA.
[‡]Assistant Professor, Department of Aerospace Engineering, University of Illinois Urbana-Champaign, USA, AAS/AIAA Member.
[§]Assistant Professor, Department of Aerospace Engineering and Coordinated Science Laboratory, University of Illinois Urbana-Champaign, USA.
[*]https://rogue.space/orbots/

is typically handled through *passive abort strategies*[10] where no thrust is used. In contrast, our approach belongs to *active safety* methods[9,10] where the remaining controlled thrusters are employed to ensure safety. However, our malfunctioning thrusters are not disabled, but instead they do not respond to the controller and fire randomly. Hence, we cannot use classical active safety methods.[9,10] Instead, we adopt the *resilience* framework[6,11,12] by assuming the presence of thrust sensors, thus enabling the implementation of fault-detection and isolation methods.[13,14]

Because of the reaction times of the sensors and thrusters,[14] the controller cannot counteract the undesirable thrust in real-time. Our objective is then to demonstrate that the inspection mission can be carried out safely despite the malfunctioning thruster and the actuation delays. More specifically, we want the damaged spacecraft to accurately follow a safe minimal-fuel reference trajectory. We generate this trajectory with a convex algorithm[15] relying on second-order cone programming methods whose main advantages are their reliability and speed of execution while not requiring any user-supplied initial guess.[16]

As the current state of resilience theory does not yet account for actuation delay and trajectory tracking after the loss of control over an actuator, we need to establish further safety guarantees in addition to those provided by resilience. More specifically, we want to prevent the malfunctioning spacecraft from entering the keep-out sphere surrounding the target satellite. To do so, we calculate the minimal stopping distance for the malfunctioning spacecraft and feed this additional safety constraint to the convex optimization method[15] to generate an updated reference trajectory. This trajectory is then tracked by the malfunctioning spacecraft thanks to a Proportional Integral Derivative (PID)[17] adaptive controller.[18] To compensate for the sensing and actuation delays we upgrade the controller with a state predictor.[19–21]

The main contributions of this work are twofold. Firstly, we establish the resilience of a spacecraft with nonlinear dynamics. Secondly, we demonstrate that on-orbit inspection can be performed safely despite a loss of control over one thruster of an adequately overactuated spacecraft. The remainder of this paper is structured as follows. First, we introduce our problem of interest and the relative dynamics of the satellites. In the second section we apply resilience theory to our malfunctioning spacecraft to demonstrate its remaining capabilities. The following section is dedicated to ensuring safety by keeping the reference trajectory far enough from the keep-out sphere. Afterwards, we detail the controller design and the results of the numerical simulations. The final sections provide concluding remarks, future work ideas and the notations necessary for our theory.

PROBLEM STATEMENT

We consider two spacecrafts on circular orbit around Earth and we focus on the chaser spacecraft, whose mission is to inspect the other spacecraft, the target. More specifically, we are interested by the proximity operations of the inspection mission, so we employ the Clohessy-Wiltshire equations in a local-vertical, local-horizontal frame.[15] The state vector $X = \begin{pmatrix} x & y & z & \dot{x} & \dot{y} & \dot{z} \end{pmatrix} \in \mathbb{R}^6$ represents the difference in position and velocity between the two spacecrafts and initially follows the dynamics

$$\dot{X}(t) = AX(t) + r\bar{B}\bar{u}(t), \qquad X(0) = X_0 \in \mathbb{R}^6, \tag{1}$$

with $\bar{u} = \begin{pmatrix} \bar{u}_1 & \bar{u}_2 & \bar{u}_3 & \bar{u}_4 & \bar{u}_5 \end{pmatrix}$ the input of the five thrusters, $\bar{u}_i \in [0, 1]$, and a *thrust-to-weight ratio* $r = 1.5 \times 10^{-4}\, m/s^2$, as we consider a spacecraft of mass $600\, kg$ and five PPS-1350 thrusters of maximal thrust $90\, mN$.[22] Note that in the Clohessy-Witshire equations the z-dynamics are decoupled from the other two axis as $\ddot{z}(t) = -\Omega^2 z(t) + r\bar{B}_z\bar{u}(t)$, with $\Omega = 0.00106\, s^{-1}$ the mean orbital rate of

the target's orbit, chosen to match that of the Restore-L mission.[5] Hence, we focus on the two-dimensional dynamics in the (x, y)-plane, with the following matrices:

$$A = \begin{bmatrix} 0 & 0 & 1 & 0 \\ 0 & 0 & 0 & 1 \\ 3\Omega^2 & 0 & 0 & 2\Omega \\ 0 & 0 & -2\Omega & 0 \end{bmatrix} \quad \text{and} \quad \bar{B} = \begin{bmatrix} 0 & 0 & 0 & 0 & 0 \\ 0 & 0 & 0 & 0 & 0 \\ 1 & 1 & -1 & -\sqrt{2} & -1 \\ 1 & -1 & -1 & 0 & 1 \end{bmatrix}.$$

The thrusters are rigidly fixed on the spacecraft and are aligned with its center of mass, as illustrated on Figure 1, so that they do not create any torque.[9] The attitude of the spacecraft is controlled by an independent system of reaction wheels so that the camera is always pointing at the target during the inspection mission as shown on Figure 1. As a result, the relative dynamics lose their linearity to become

$$\dot{X}(t) = AX(t) + rR_\theta \bar{B}\bar{u}(t), \qquad \text{with} \qquad R_\theta = \begin{bmatrix} 1 & 0 & 0 & 0 \\ 0 & 1 & 0 & 0 \\ 0 & 0 & \cos(\theta) & -\sin(\theta) \\ 0 & 0 & \sin(\theta) & \cos(\theta) \end{bmatrix}, \tag{2}$$

where θ is illustrated on Figure 1 and is defined as $\theta(t) = \arctan\left(\frac{y(t)}{x(t)}\right)$.

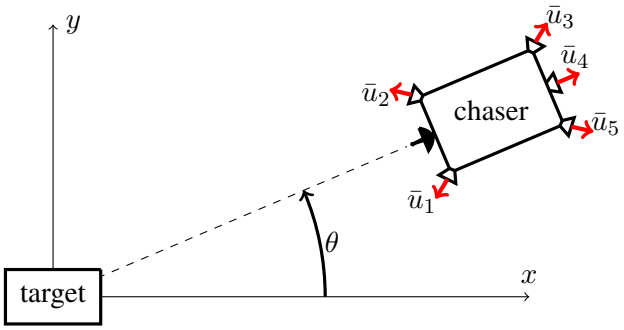

Figure 1: Relative positions and attitudes of the two satellites, with the camera of the chaser always pointing at the target.

After an error in the on-board computer[7] of the chaser satellite, the controller loses control authority over one of the thrusters. The input signal $\bar{u}(\cdot)$ is then split between the undesirable signal $w(\cdot) \in \mathcal{W} = [0, 1]$ and the controlled signal $u(\cdot) \in \mathcal{U} = [0, 1]^4$. Matrix $\bar{B}$ is accordingly split into two constant matrices $B \in \mathbb{R}^{4\times4}$ and $C \in \mathbb{R}^4$ so that the dynamics become

$$\dot{X}(t) = AX(t) + rR_\theta Bu(t) + rR_\theta Cw(t). \tag{3}$$

Due to its location shown on Figure 1, thruster 4 plays a special role in the actuation of the chaser spacecraft. Then, in this work, we focus on the loss of control over thruster 4, so that

$$B = \begin{bmatrix} 0 & 0 & 0 & 0 \\ 0 & 0 & 0 & 0 \\ 1 & 1 & -1 & -1 \\ 1 & -1 & -1 & 1 \end{bmatrix} \quad \text{and} \quad C = \begin{bmatrix} 0 \\ 0 \\ -\sqrt{2} \\ 0 \end{bmatrix}. \tag{4}$$

In order to account for the sensors and thrusters delays,[13,14] we assume that the input signal operates with a constant input delay $\tau = 1\,s$ so that the dynamics are in fact

$$\dot{X}(t) = AX(t) + rR_\theta Bu\big(t, X(t-\tau), w(t-\tau)\big) + rR_\theta Cw(t). \tag{5}$$

Having described the relevant dynamics, we now focus on the reference trajectory that our malfunctioning satellite needs to follow to perform its inspection mission. Following the Restore-L protocol,[5] we assume that the satellite must come within $80\,m$ of the target for a precise inspection. Hence, we want the satellite to occupy successively the 5 following holding points $(0, 80)$, $(-80, 0)$, $(0, -80)$, $(80, 0)$ and $(0, 80)$, while starting from $X_0 = (0, 200)$. Using a convex optimization method[15] we compute on Figure 2 the minimal fuel trajectory linking these waypoints with 90 minutes transfers for the undamaged satellite. For safety considerations, we consider a keep-out sphere (KOS) of radius $R_{KOS} = 50\,m$ around the target as in the Restore-L mission[5] and we also limit the relative velocity of the spacecrafts $\sqrt{\dot{x}(t)^2 + \dot{y}(t)^2} \leq V_{max} = 5\,cm/s$ as in benchmark problems.[23,24]

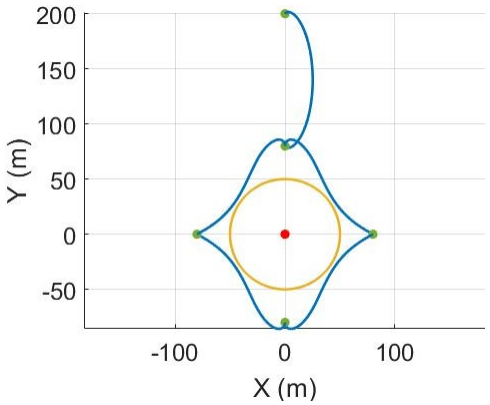

Figure 2: Reference minimal-fuel trajectory (blue) linking the 5 waypoints (green) to inspect the target satellite (red) without breaching the KOS (yellow).

We can then formulate our problem of interest.

Problem 1. *Verify whether the satellite can follow the reference trajectory and respect the safety constraints after enduring a loss of control authority over thruster 4.*

SPACECRAFT RESILIENCE

Let us now investigate whether the chaser spacecraft can complete its mission despite the loss of control over thruster 4 relying on *resilience theory*.[25]

Definition. *System* (2) *is* resilient *to the loss of control over one of its thrusters if for any target* X_{goal} *and any undesirable signal* $w(\cdot) \in \mathcal{W}$ *there exists a control signal* $u(\cdot) \in \mathcal{U}$ *such that the resulting malfunctioning system* (3) *can reach* X_{goal}.[25]

According to Hájek's duality theorem,[26] resilience of system (2) is equivalent to *controllability* of system

$$\dot{X}(t) = AX(t) + rR_\theta p(t), \qquad p \in \mathcal{P}, \tag{6}$$

where the input set $\mathcal{P} := \mathcal{BU} \ominus (-\mathcal{CW}) = \{p \in \mathcal{BU} : p - Cw \in \mathcal{BU} \text{ for all } w \in \mathcal{W}\}$ is the Minkowski difference between the set of control inputs $\mathcal{BU} = \{Bu : u \in \mathcal{U}\}$ and the opposite of the set of undesirable inputs $-\mathcal{CW} = \{-Cw : w \in \mathcal{W}\}$. Then, $\mathcal{P}$ represents the amount of control authority remaining after counteracting the worst undesirable input. For the reader's convenience, we provide the definition of controllability.[27]

Definition. *System* (6) *is* controllable *if for all* $X_0 \in \mathbb{R}^4$ *and all* $X_{goal} \in \mathbb{R}^4$*, there exists a time* T *and a control signal* $p(\cdot) \in \mathcal{P}$ *driving the state of system* (6) *from* $X(0) = X_0$ *to* $X(T) = X_{goal}$*.*

With matrices B and C from Eq. (4), $\mathcal{BU}$ and $-\mathcal{CW}$ are polytopes in $\mathbb{R}^4$, but they are both of dimension 2, so they can be represented as the blue and red polygons in Figure 3.

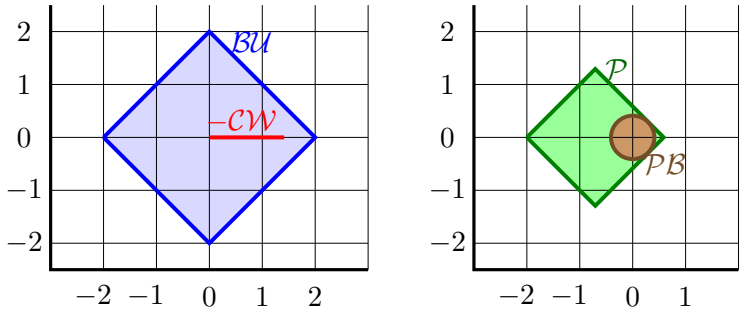

Figure 3: Illustration of polygons $\mathcal{BU}$ (blue), $-\mathcal{CW}$ (red), their Minkowski difference $\mathcal{P}$ (green) and the largest ball $\mathcal{PB}$ (brown) centered on 0 fitting inside $\mathcal{P}$ for the loss of thruster 4.

Proposition 1. *System* (2) *is resilient to the loss of control over thruster 4.*

Proof. To prove the resilience of system (2), by Hájek's duality theorem[26] it suffices to prove that system (6) is controllable. However, controllability of nonlinear systems is generally a difficult problem.[28] To handle the nonlinearity caused by the rotation R_θ in system (6), we will construct a related linear time-invariant system, namely system (7), whose controllability implies that of system (6).

Because $-\mathcal{CW}$ is strictly included in $\mathcal{BU}$, the origin belongs in the interior of polygon $\mathcal{P}$, as seen on Figure 3. Then, we can define $p_{min} > 0$ as the radius of the largest ball centered on 0 and fitting inside $\mathcal{P}$ as $p_{min} := \min\{\|p\| : p \in \partial\mathcal{P}\}$. In our case $p_{min} = \sqrt{2} - 1 = 0.414$. Then, the ball $\mathcal{PB} := \{p : \|p\| \leq p_{min}\}$ is a subset of $\mathcal{P}$ as illustrated on Figure 3. Consider system (6) but restrain inputs to $\mathcal{PB}$. Because $\mathcal{PB}$ is a ball, there is a one-to-one correspondence between inputs $p \in \mathcal{PB}$ and $R_\theta p \in \mathcal{PB}$, so the dynamics of system (6) with inputs constrained to $\mathcal{PB}$ are in fact

$$\dot{X}(t) = AX(t) + r\hat{B}p(t), \qquad p \in \mathcal{PB} \subset \mathbb{R}^2, \qquad \hat{B} = \begin{bmatrix} 0_{2\times 2} \\ I_2 \end{bmatrix}. \tag{7}$$

Because the first two rows of B and C defined in Eq. (4) are null, the geometrical work we completed above only concerns the last two coordinates of the inputs, which explains the structure of matrix $\hat{B}$. To prove the controllability of system (7), we verify the conditions of Corollary 3.7 of Reference 27:

- $0 \in \mathcal{PB}$, so taking $p = 0$ makes $\hat{B}p = 0$;
- since $p_{min} > 0$ and $\mathcal{PB}$ is convex, its convex hull has a non-empty interior in $\mathbb{R}^2$;

- $[\hat{B}, A\hat{B}] = \begin{bmatrix} 0_{2\times 2} & I_2 \\ I_2 & * \end{bmatrix}$, so $\operatorname{rank}([\hat{B}, A\hat{B}]) = 4$, the controllability matrix has full rank;
- the only real eigenvector of $A^\top$ is $v = (2\Omega, 0, 0, 1)$, which makes $v^\top \hat{B} p = p_2$ for all $p = (p_1, p_2) \in \mathcal{PB}$ and p_2 can be chosen positive or negative since $p_{min} > 0$;
- the eigenvalues of A are $\{0, 0, \pm j\Omega\}$, so they all have a zero real part.

Hence, system (7) is controllable.[27] Because system (6) follows the same dynamics as (7), and has a larger input set encompassing that of system (7), it is also controllable. Then, according to Hájek's duality theorem[26] system (2) is resilient to the loss of control over thruster 4. □

Remark. *The loss of control over a thruster other than 4 leads to a polygon $\mathcal{P}$ with $(0, 0)$ on its boundary. Then, there is no ball $\mathcal{PB}$ as above, so the nonlinear dynamics* (6) *cannot be linearized into* (7)*, which renders the resilience study considerably more complex. We keep this study for future work. Note that adding a sixth thruster instead of the camera (see Figure 1) would guarantee resilience to the loss of any single thruster.*

Proposition 1 shows that despite the loss of control authority over thruster 4, the spacecraft can still reach any target. However, the current results from resilience theory do not deal with actuation delay and trajectory tracking. Hence, Proposition 1 is only a necessary condition for the answer to Problem 1 to be affirmative. To ensure the safety of the target satellite, we proceed to modify the reference trajectory to maintain a greater distance between both satellites.

SAFE REFERENCE TRAJECTORY

To prevent the chaser spacecraft from breaching the KOS while operating with a malfunctioning thruster, we want the reference trajectory to remain further away from the target while keeping the same waypoints to complete the mission. To quantify the trajectory modification, we calculate the stopping distance for the malfunctioning spacecraft when it is initially traveling at the maximal allowed velocity $V_{max} = 5\, cm/s$. Then, we increase the radius of the KOS by this stopping distance to prevent the spacecraft from entering the initial KOS.

Proposition 2. *After the loss of control over thruster 4, if the radius of the KOS is increased by $20.2\, m$, the controller can prevent all trajectories from reaching the initial KOS when their initial velocity is smaller than V_{max}.*

Proof. The dynamics of system (7) are $\ddot{x} = 3\Omega^2 x + 2\Omega\dot{y} + r p_x$ and $\ddot{y} = -2\Omega\dot{x} + r p_y$. Note that the term $3\Omega^2 x$ is repulsive, i.e., if $x > 0$, then $3\Omega^2 x > 0$, making $\dot{x}$ increase, which causes x to increase and thus pushing the spacecraft further from the KOS, and conversely if $x < 0$ the term $3\Omega^2 x$ makes x decrease. Hence the term $3\Omega^2 x$ brings additional safety and can be neglected without endangering the spacecraft. Then, the simplified velocity dynamics become $\dot{v} = A_v v + rp$, with $v = (\dot{x}\ \dot{y})$, $p \in \mathcal{PB}$ and $A_v = \begin{bmatrix} 0 & 2\Omega \\ -2\Omega & 0 \end{bmatrix}$. We want to bring the velocity v to zero before breaching the KOS, so we study the dynamics

$$\frac{d}{dt}\|v\|^2 = \dot{v}^\top v + v^\top \dot{v} = v^\top \big(A_v^\top + A_v\big) v + 2v^\top r p = 2v^\top r p,$$

because $A_v^\top = -A_v$. We choose to apply the control $p = -\frac{v}{\|v\|} p_{min} \in \mathcal{PB}$ for $v \neq 0$. Then, we have a differential equation specifying the rate at which we can reduce the velocity: $\frac{d}{dt}\|v\|^2 = -2r p_{min}\|v\|$. The non-trivial solution to this differential equation is $\|v(t)\| = \|v(0)\| - r p_{min} t$.

Since the initial velocity $\|v(0)\|$ is limited by $V_{max} = 5\,cm/s$, the maximal stopping time is $T = \frac{V_{max}}{rp_{min}}$. By integrating the velocity we evaluate the maximal stopping distance:

$$\int_0^T \|v(t)\|\,dt = \int_0^T (V_{max} - rp_{min}t)\,dt = V_{max}T - rp_{min}\frac{T^2}{2} = \frac{V_{max}^2}{2rp_{min}}.$$

To account for the actuation delay τ during which the spacecraft can travel for τ seconds unnnoticed by the controller, we add an extra τV_{max} to the safety distance. Hence, we need to increase the radius of the KOS by $\tau V_{max} + \frac{V_{max}^2}{2rp_{min}} = 20.2\,m$. □

To verify the safety guarantees of the increased KOS, we illustrate a worst-case scenario by computing several trajectories starting on the boundary of the increased KOS with an initial velocity V_{max} pointing towards the target. Because the malfunctioning thruster acceleration vector always points towards the target ($\bar{u}_4$ in Figure 1), the worst undesirable input is $w = 1$. Based on the thruster geometry illustrated in Figure 1, we choose the counteracting control input $\bar{u}_1 = \bar{u}_2 = 1$ and $\bar{u}_3 = \bar{u}_5 = 0$. The resulting trajectories are propagated until they turn around, and none of them reach the initial KOS, as pictured on Figure 4(a). Proceeding with the proof of Proposition 2 without making use of the repulsive term $3\Omega^2 x$ made our increased KOS more conservative, which is why none of the trajectories of Figure 4(a) even come close to the initial KOS.

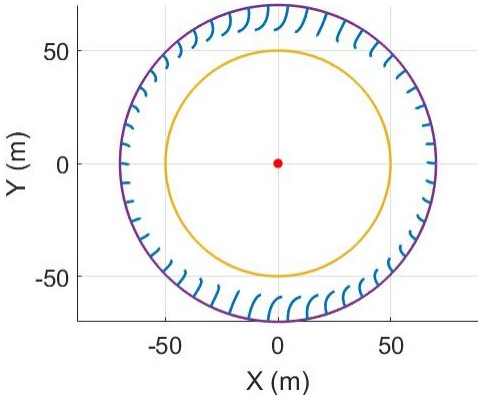

(a) Worst-case trajectories (blue) starting from the increased KOS (purple) with initial velocity V_{max} pointing towards the target (red) all turn around before reaching the initial innermost KOS (yellow).

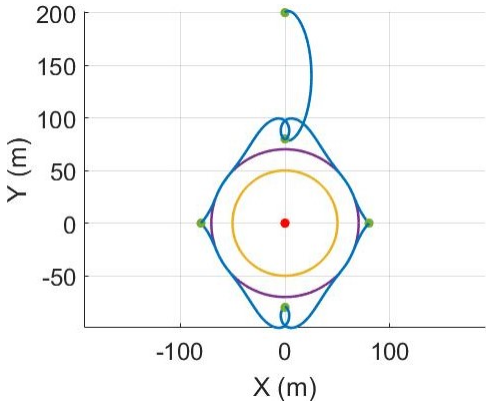

(b) Reference minimal-fuel trajectory (blue) with 5 waypoints (green) to inspect the target satellite (red) without breaching the increased KOS (purple).

Figure 4: Safety guarantees with respect to the initial KOS (yellow) by considering an increased KOS (purple).

Now that we have increased the KOS, we need to update the reference trajectory accordingly. Indeed, the initial reference trajectory pictured on Figure 2 comes too close from the initial KOS and is actually partially inside the increased KOS. We update the reference trajectory using the same convex method[15] as previously and it becomes tangent to the increased KOS, as shown in Figure 4(b).

Let us now analyze this updated reference trajectory. Because the chaser is constantly pointing its camera towards the target, its orientation angle θ (see Figure 1) varies throughout the trajectory as shown on Figure 5(a) and starts at $\theta(0) = 90°$ since the initial position of the spacecraft is on the y-axis, as illustrated in Figure 4(b).

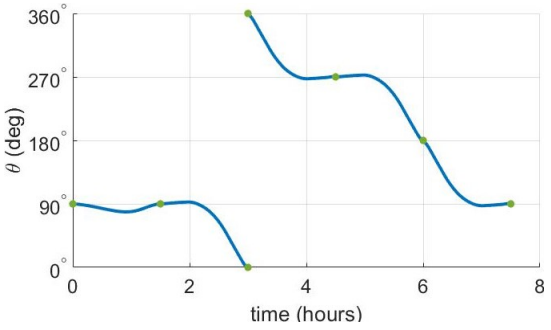

(a) Orientation of the chaser θ during its mission, with the waypoints in green.

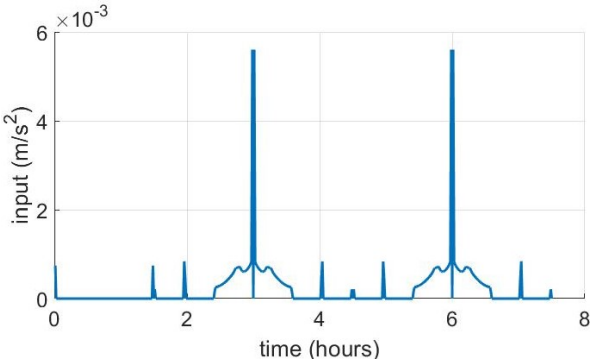

(b) Magnitude of the reference input signal $\|u_r\|$.

Figure 5: Chaser orientation and thrust profile for the reference trajectory.

When the undamaged satellite follows the updated reference trajectory of Figure 4(b), the resulting minimal-fuel thrust profile is represented on Figure 5(b) and shows several impulses. Their symmetry comes from the symmetry of the reference trajectory shown in Figure 4(b). To gain insight into the location and magnitude of each thrust impulse, we relate them with the trajectory on Figure 6.

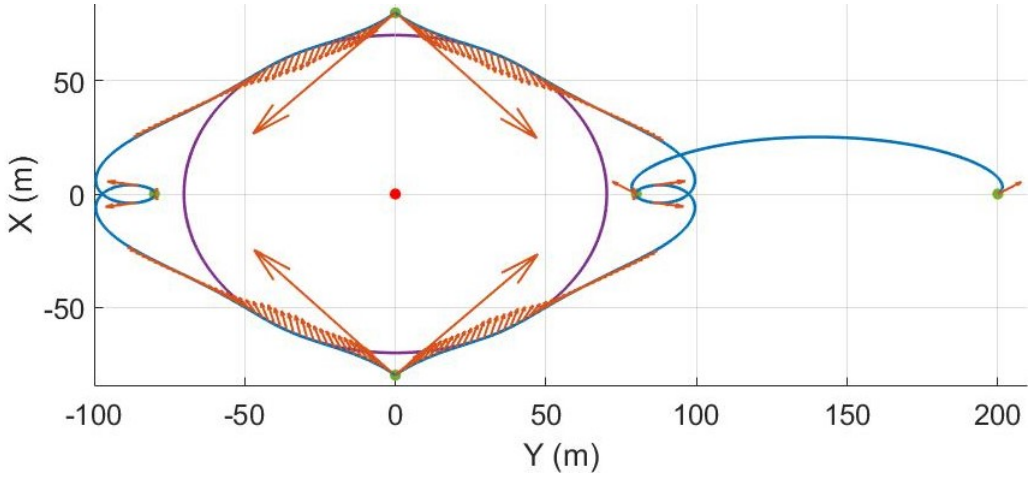

Figure 6: Reference trajectory (blue) with thrust impulses (red arrows).

The first impulse in Figure 5(b) places the spacecraft on the first leg of its transfer starting at $y = 200\,m$ in Figure 6. Each one of the two largest spikes of Figure 5(b) is in fact composed of two thrust impulses represented by the largest arrows on Figure 6. These impulses are used to stop and restart from the two waypoints situated at $y = 0\,m$ on Figure 6. Surrounding the largest spikes, Figure 5(b) shows two intervals of continuous thrust, whose goal is to maintain the trajectory tangent to the increased KOS, as illustrated by the continuous range of arrows in Figure 6 between $y = -50\,m$ and $y = 50\,m$.

Having updated our reference trajectory to guarantee safety of the initial KOS, we now need to design a controller able to track this trajectory despite malfunctioning thruster 4 and the actuation delay.

CONTROLLER DESIGN FOR THE MALFUNCTIONING SPACECRAFT

To mitigate the effects of the actuation delay on the malfunctioning spacecraft, we choose to use the state predictor $X_p(t)$ from Léchappé,[21] which is based on the Artstein predictor.[19,20] The objective of the predictor $X_p(t)$ is to estimate the state $X(t+\tau)$ based on the information available at time t, so that the controller can anticipate and somewhat compensate its delay $\tau > 0$. Given the system's dynamics (5), we take

$$X_p(t) = e^{A\tau}X(t) + \int_{t-\tau}^{t} e^{A(t-s)} r R_\theta \big(Bu(s) + Cw(s)\big) ds. \tag{8}$$

To follow as closely as possible the fuel-optimal reference trajectory (X_{ref}, u_{ref}) pictured in Figure 4(b) despite the undesirable inputs w, we use adaptive trajectory tracking[18] with the state predictor X_p, resulting in the following control law:

$$u(t) = u_{ref}(t) + K_\theta\big(X_{ref}(t) - X_p(t)\big). \tag{9}$$

Matrix K_θ is a function of θ chosen to make matrix $A - rR_\theta BK_\theta$ Hurwitz at all θ. To enforce the input constraint $u_i(t) \in [0,1]$, we add a saturation on the control input u. Let us also define the state error as $\Delta(t) := X_{ref}(t) - X_p(t)$ to be minimized during tracking. Then, controller (9) relies on a simple proportional error feedback to ensure the convergence of predictor X_p to reference X_{ref}. This controller does not perform as well as desired. Indeed, the tracking trajectory exhibits an ever growing position error as shown on Figure 7. We can see on Figure 7(a) that the tracking trajectory (red) moves further away from the reference (blue) as the orbit progresses clockwise.

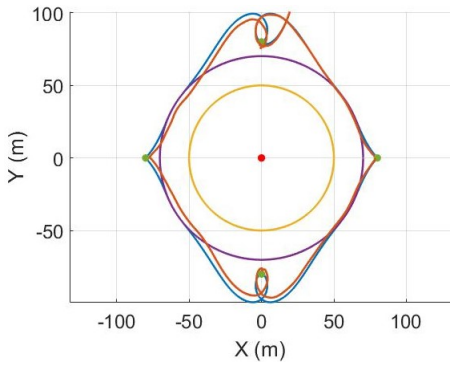

(a) Tracking trajectory (red) moving further away from the reference (blue).

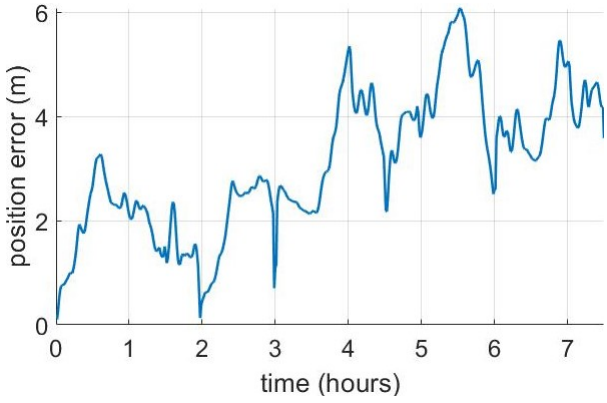

(b) Ever growing position error of the tracking trajectory.

Figure 7: Proportional controller (9) yields a growing position error during trajectory tracking.

To improve the tracking performance of the spacecraft, we upgrade controller (9) to a Proportional Integral Derivative (PID) controller:[17]

$$u(t) = u_{ref}(t) + K_\theta \left(k_p \Delta(t) + k_i \int_0^t \Delta(s)\, ds + k_d \frac{d}{dt}\Delta(t) \right), \tag{10}$$

where k_p, k_i and k_d are scalar gains to be tuned. Then, control law (10) often ensures excellent tracking of the reference trajectory X_{ref}, but is not successful at making the state $X(t)$ converge to the waypoint X_{goal} as illustrated on Figure 8. To remedy this issue, when the trajectory is close

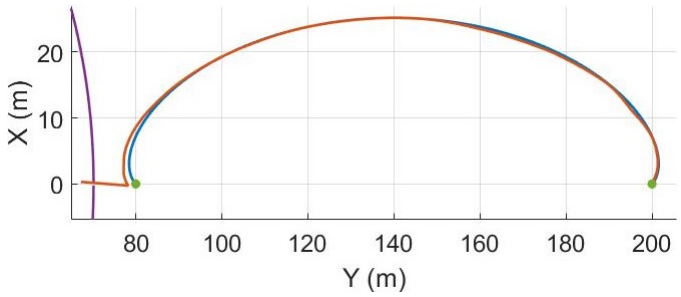

Figure 8: First leg of the trajectory tracking (red) following the reference trajectory (blue). The tracking does not converge to the leftmost waypoint X_{goal} (green) at $y = 80$ m.

enough to X_{goal}, we replace $\Delta(t)$ in control law (10) by $\Delta_g(t) := X_{goal} - X_p(t)$. For the switching to happen even if the undesirable inputs prevent perfect tracking, we choose to switch when the reference trajectory gets within $1\,m$ of the waypoint.

We now implement this controller and track the reference trajectory in the presence of undesirable thrust inputs and actuation delays.

NUMERICAL SIMULATION

As shown in Figure 4(b), the reference trajectory is tangent to the increased KOS. Hence, we need almost perfect tracking in order not to violate the increased KOS. With the controller designed in the previous section, we simulate the tracking of the reference trajectory and we observe on Figure 9 that the tracking trajectory barely enters the increased KOS.

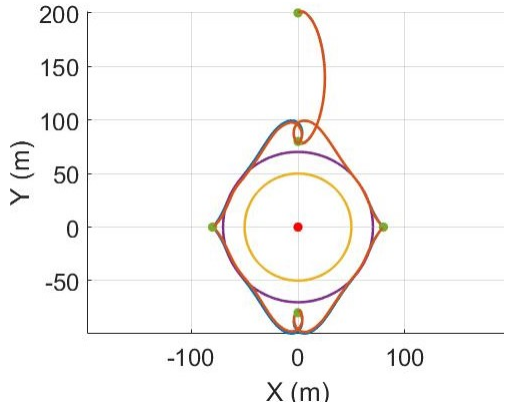

Figure 9: Trajectory tracking (red) of the reference trajectory (blue) despite actuation delay and loss of control authority over thruster 4.

After tuning experiments, the values of the PID gains for our simulations are $k_p = 1.4$, $k_i = 1.4 \times 10^{-4}$ and $k_d = 42$. Matrix K_θ is computed on MATLAB as $K_\theta = lqr(A, R_\theta B, Q, R)$ with Q and R two identity matrices of appropriate sizes. We now analyze the performance of the tracking on Figure 10. We compute the position error between the reference state and the tracking state on Figure 10(a) and we observe that the error is never larger than $3.5\,m$. The velocity tracking is also successful, as illustrated on Figure 10(b).

Note that the reference trajectory is computed by solving a convex optimization problem,[15] where we specify constraints on the thrust inputs $u_i(t) \in [0, 1]$, the velocity $v(t) \leq v_{max}$ and the position

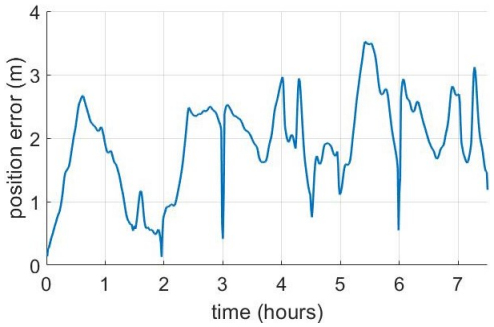

(a) Position error between the reference trajectory and the tracking trajectory.

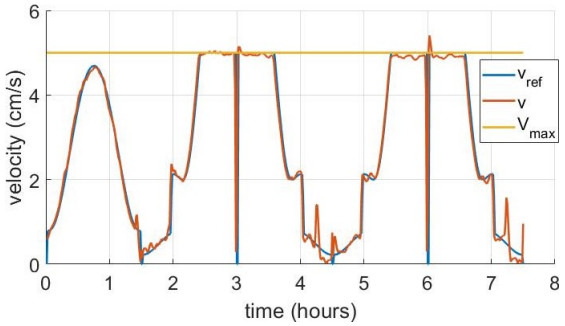

(b) Velocity comparisons for the reference trajectory v_{ref} (blue), tracking trajectory v (red) and the maximal velocity allowed V_{max} (yellow).

Figure 10: Analysis of the trajectory tracking performance.

$\left\|\left(x(t)\ y(t)\right)\right\| > R_{KOS}$. This last constraint is not convex, but Reference 15 details how to handle it. On the other hand, the tracking trajectory is only designed through the controller detailed in the previous section. The thrust bounds are applied a posteriori through a saturation. Enforcing velocity constraints with a control law only affecting the acceleration would lead to an overly complex controller. Thus, only the good performance of the reference tracking method is responsible for the trajectory to predominantly respect the increased KOS and the maximal velocity.

The undesirable input w is generated as a continuous stochastic signal, whose magnitude is represented in yellow in Figure 11(a). To counteract w, the controlled inputs u naturally do not follow exactly the reference input u_{ref} so that the thrust profile of the tracking trajectory cannot be qualified of impulsive, on the contrary to Figure 5(b). We note however, that u has the same two large spikes as u_{ref}, which are produced by thruster 3 and 5 according to Figure 11(b) and correspond to the largest arrows in Figure 6.

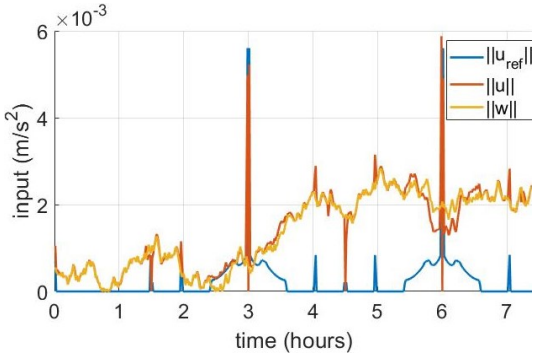

(a) Magnitude of the thrust inputs for the reference trajectory $\|u_{ref}\|$ (blue), for the tracking trajectory the controlled input is $\|u\|$ (red) and the undesirable input is $\|w\|$ (yellow).

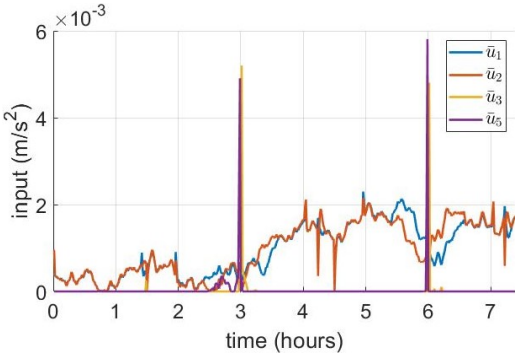

(b) Thrust profiles for the four controlled thrusters of the chaser satellite on the tracking trajectory.

Figure 11: Analysis of the thrust profile of the malfunctioning satellite.

Figure 12 shows the fuel consumption on the reference trajectory and on the tracking trajectory. The yellow curve represents the fuel used to produce the undesirable input, while the red one shows the fuel used by the controlled thrusters. In the scenario depicted on Figure 12, the controlled thrusters use $0.54\,kg$ of fuel to follow the reference trajectory while counteracting the

malfunctioning thruster, which uses $0.42\,kg$ of fuel. The reference scenario, where no thruster is malfunctioning, leads to a fuel use of $0.21\,kg$.

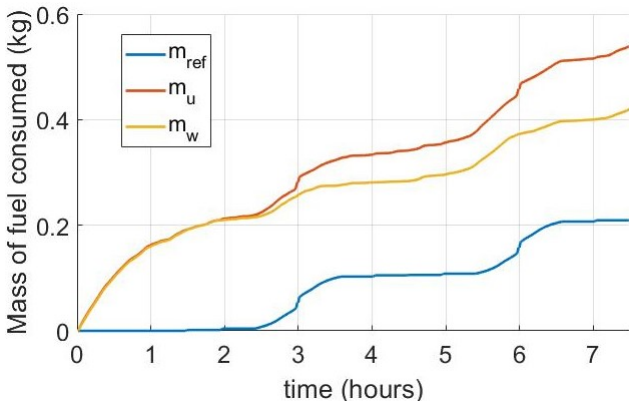

Figure 12: Comparison of fuel consumption. The mass of fuel used to complete the reference trajectory is m_{ref} (blue). After the malfunction, the controlled thrusters use a mass of fuel m_u (red), while the malfunctioning thruster consumes a mass m_w (yellow).

We now proceed to a Monte-Carlo simulation to test the reliability of our approach. We generate a thousand stochastic undesirable thrust signals w in the interval $[0,\ 3]\,mm/s^2$, so that their magnitude is similar to that of the control signals as shown on Figure 11(a). Then, we implement our controller to track the reference trajectory despite these undesirable thrust signals.

The adaptive PID controller developed in this work is very reliable as demonstrated by Figure 13(a), where we can see that the tracking trajectories follow their reference and barely enter the increased KOS. Indeed, over the thousand runs of the Monte Carlo simulation, the maximal penetration inside the increased KOS is always less than $2.44\,m$, which is a far cry from the $20.2\,m$ necessary to breach the inner KOS. The velocity profile of the tracking trajectory as shown on Figure 13(b) is also barely affected by the variations of w.

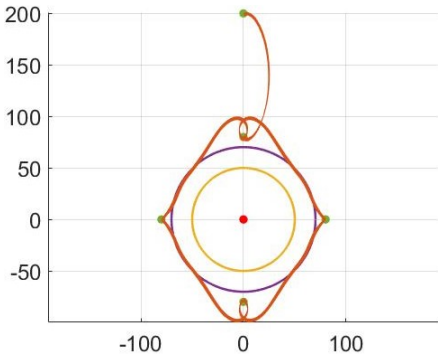

(a) Tracking trajectories (red) of the Monte Carlo simulation.

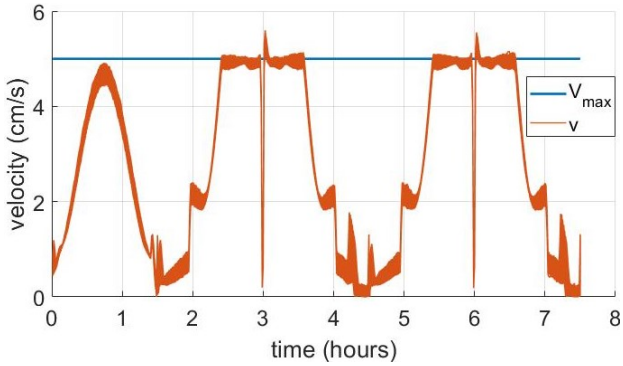

(b) Velocity profile of the multiple tracking trajectories.

Figure 13: Trajectory tracking analysis of the Monte Carlo simulation.

While the trajectory and the velocity are barely modified by the changes of w, the position error and fuel consumption are more effected by these changes as shown on Figure 14. Despite their wider distribution, the maximal position error of each trajectory stays contained, never more than $4.75\,m$ away from the reference position, as illustrated on Figure 14(a). Figure 14(b) shows the

difference of the fuel consumption between the controlled thrusters and the malfunctioning one. A negative difference states that the controlled thrusters require less fuel than the malfunctioning one. The worst-case scenario of the Monte Carlo simulation shows a maximal difference of fuel use of $0.19\,kg$, which is slightly less than the reference fuel used m_{ref} as shown in Figure 12. The intuition in the worst-case scenario is that the controlled thrusters need to use the same amount of fuel as the malfunctioning one to counteract it plus m_{ref} to track the reference trajectory. Since these two tasks potentially overlap, the differences shown on Figure 14(b) are all smaller than $m_{ref} = 0.21\,kg$.

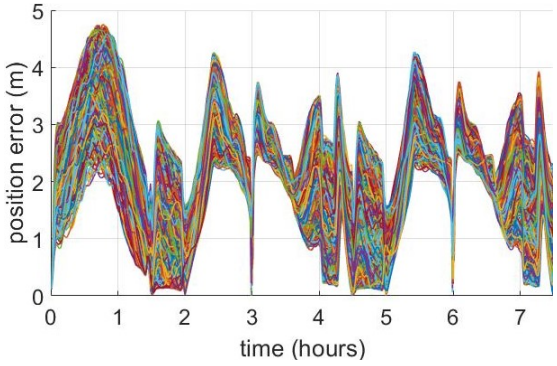

(a) Position error between the reference trajectory and the multiple tracking trajectories.

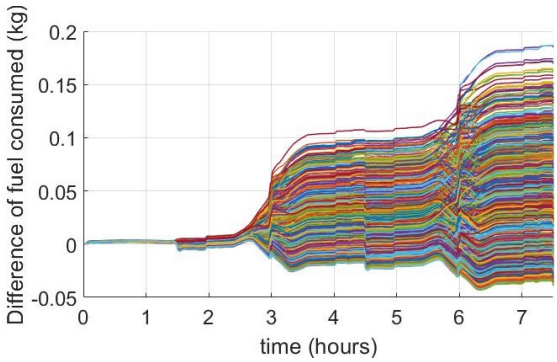

(b) Difference of fuel consumption between the controlled thrusters and the malfunctioning one.

Figure 14: Position error and distribution of the fuel consumption difference of the Monte Carlo simulation.

As evident on Figure 13(b), the tracking velocity tends to overshoot the reference velocity when it increases quickly, like at time $3\,h$ and $6\,h$. To quantify the overshot of V_{max}, we generated the probability distribution of the maximal velocity reached during the tracking trajectory over the Monte Carlo simulation. Figure 15(a) shows that in the vast majority of cases the maximal velocity does not exceeds $5.1\,cm/s$. Additionally, the velocity exceeds V_{max} only for small percentages of the mission time as illustrated by Figure 15(b). The Monte Carlo simulation then shows that our controller enables a safe inspection mission to be performed despite the malfunctioning thruster 4 and the actuation delays.

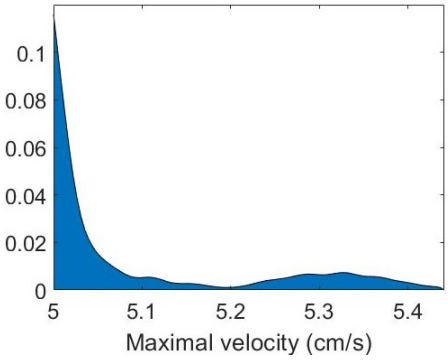

(a) Probability distribution of the maximal velocity of the tracking trajectory.

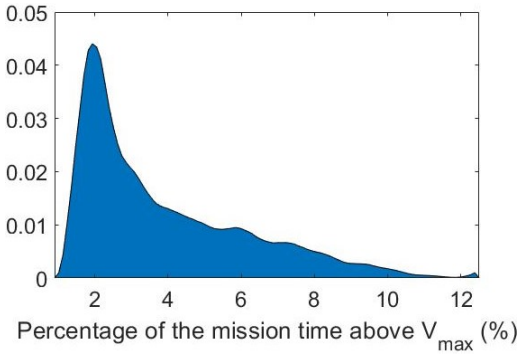

(b) Probability distribution of the percentage of the mission time spent at velocities higher than V_{max}.

Figure 15: Probability distributions of the velocity from the Monte Carlo simulation.

CONCLUSION AND FUTURE WORK

We presented a new methodology to safely perform a satellite inspection mission despite actuation delays and the loss of control authority over a thruster. To mitigate these issues, we based our approach on predictors and resilience theory. The proposed control law for a malfunctioning spacecraft relies on adaptive trajectory tracking to follow the safe reference trajectory computed with a convex solver. The results show that the tracking is accurate despite undesirable thrust of similar magnitude as that of the other correctly operating thrusters. Therefore, the inspection mission can be performed safely.

There are several promising avenues of future work. First, we want to formally extend resilience theory to handle actuation delay and trajectory tracking. As mentioned during the resilience analysis, we also intend to study the resilience of the spacecraft to the loss of control over its other thrusters using nonlinear systems controllability theory. Finally, we have the objective of studying the resilience of nonlinear spacecraft dynamics that combine position and attitude.

ACKNOWLEDGMENT

This work was supported by an Early Stage Innovations grant from NASA's Space Technology Research Grants Program, grant no. 80NSSC19K0209, and by NASA grant no. 80NSSC21K1030.

NOTATION

For a set $X \subseteq \mathbb{R}^n$, ∂X denotes its boundary, and its Minkowski difference with another set $Y \subseteq \mathbb{R}^n$ is denoted as $X \ominus Y := \left\{ z \in \mathbb{R}^n : z + y \in X \text{ for all } y \in Y \right\}$. We use I_n to denote the identity matrix of size n and $0_{n \times m}$ to denote the null matrix with n rows and m columns.

REFERENCES

[1] D. C. Woffinden, "On-orbit satellite inspection: navigation and Δv analysis," Master's thesis, Massachusetts Institute of Technology, 2004.

[2] N. M. Horri, K. U. Kristiansen, P. Palmer, and M. Roberts, "Relative attitude dynamics and control for a satellite inspection mission," *Acta Astronautica*, Vol. 71, 2012, pp. 109 – 118.

[3] J. Diaz and M. Abderrahim, "Visual inspection system for autonomous robotic on-orbit satellite servicing," *9th ESA Workshop on Advanced Space Technologies for Robotics and Automation*, 2006.

[4] T. M. Silva, J.-B. Bouvier, K. Xu, M. Hirabayashi, and K. Ho, "Spacecraft trajectory tracking and parameter estimation around a splitting contact binary asteroid," *Acta Astronautica*, Vol. 171, 2020, pp. 280 – 289.

[5] M. A. Vavrina, C. E. Skelton, K. D. DeWeese, B. J. Naasz, D. E. Gaylor, and C. D'souza, "Safe rendezvous trajectory design for the Restore-L mission," *29th AAS/AIAA Space Flight Mechanics Meeting*, 2019, pp. 3649 – 3668.

[6] J.-B. Bouvier and M. Ornik, "Resilient Reachability for Linear Systems," *21st IFAC World Congress*, 2020, pp. 4409 – 4414.

[7] M. Bartels, "Russia says 'software failure' caused thruster misfire at space station," *space.com*, 2021, `https://www.space.com/space-station-nauka-arrival-thruster-fire-update`.

[8] L. Y. Wang and J.-F. Zhang, "Fundamental limitations and differences of robust and adaptive control," *2001 American Control Conference*, 2001, pp. 4802 – 4807.

[9] D. A. Marsillach, S. Di Cairano, and A. Weiss, "Abort-Safe Spacecraft Rendezvous in case of Partial Thrust Failure," *59th IEEE Conference on Decision and Control*, 2020, pp. 1490 – 1495.

[10] L. Breger and J. How, "Safe trajectories for autonomous rendezvous of spacecraft," *Journal of Guidance, Control, and Dynamics*, Vol. 31, No. 5, 2008, pp. 1478 – 1489.

[11] J.-B. Bouvier and M. Ornik, "Designing Resilient Linear Systems," *IEEE Transactions on Automatic Control*, Vol. 67, No. 9, 2022, pp. 4832 – 4837.

[12] J.-B. Bouvier, K. Xu, and M. Ornik, "Quantitative Resilience of Linear Driftless Systems," *SIAM Conference on Control and its Applications*, 2021, pp. 32 – 39.

[13] R. J. Patton, F. J. Uppal, S. Simani, and B. Polle, "Robust FDI applied to thruster faults of a satellite system," *Control Engineering Practice*, Vol. 18, No. 9, 2010, pp. 1093 – 1109.

[14] D. Henry, "Fault diagnosis of Microscope satellite thrusters using H_∞/H_- filters," *Journal of Guidance, Control, and Dynamics*, Vol. 31, No. 3, 2008, pp. 699 – 711.

[15] N. Ortolano, D. K. Geller, and A. Avery, "Autonomous optimal trajectory planning for orbital rendezvous, satellite inspection, and final approach based on convex optimization," *Journal of the Astronautical Sciences*, Vol. 68, 2021, pp. 444 – 479.

[16] P. Lu and X. Liu, "Autonomous trajectory planning for rendezvous and proximity operations by conic optimization," *Journal of Guidance, Control, and Dynamics*, Vol. 36, No. 2, 2013, pp. 375 – 389.

[17] K. H. Ang, G. Chong, and Y. Li, "PID control system analysis, design, and technology," *IEEE Transactions on Control Systems Technology*, Vol. 13, No. 4, 2005, pp. 559 – 576.

[18] D. Bresch-Pietri and M. Krstic, "Adaptive trajectory tracking despite unknown input delay and plant parameters," *Automatica*, Vol. 45, No. 9, 2009, pp. 2074 – 2081.

[19] J.-P. Richard, "Time-delay systems: an overview of some recent advances and open problems," *Automatica*, Vol. 39, No. 10, 2003, pp. 1667 – 1694.

[20] Z. Artstein, "Linear systems with delayed controls: A reduction," *IEEE Transactions on Automatic control*, Vol. 27, No. 4, 1982, pp. 869 – 879.

[21] V. Léchappé, E. Moulay, F. Plestan, A. Glumineau, and A. Chriette, "New predictive scheme for the control of LTI systems with input delay and unknown disturbances," *Automatica*, Vol. 52, 2015, pp. 179 – 184.

[22] P. Dumazert, F. Marchandise, L. Jolivet, D. Estublier, and N. Cornu, "PPS-1350-G qualification status," *40th AIAA/ASME/SAE/ASEE Joint Propulsion Conference and Exhibit*, 2004.

[23] N. Chan and S. Mitra, "Verified hybrid LQ control for autonomous spacecraft rendezvous," *56th IEEE Conference on Decision and Control*, 2017, pp. 1427 – 1432.

[24] C. Jewison and R. S. Erwin, "A spacecraft benchmark problem for hybrid control and estimation," *55th IEEE Conference on Decision and Control*, 2016, pp. 3300 – 3305.

[25] J.-B. Bouvier and M. Ornik, "Quantitative Resilience of Linear Systems," *20th European Control Conference*, 2022, pp. 485 – 490.

[26] O. Hájek, "Duality for differential games and optimal control," *Mathematical Systems Theory*, Vol. 8, No. 1, 1974, pp. 1 – 7.

[27] R. F. Brammer, "Controllability in linear autonomous systems with positive controllers," *SIAM Journal on Control*, Vol. 10, No. 2, 1972, pp. 339 – 353.

[28] H. Sussmann and V. Jurdjevic, "Controllability of nonlinear systems," *Journal of Differential Equations*, Vol. 12, 1972, pp. 95 – 116.